ADVANCED FUNCTIONAL MATERIALS
www.afm-journal.de

Microbubble-Controlled Delivery of Biofilm-Targeting Nanoparticles to Treat MRSA Infection

Ju Yeon Chung, Yujin Ahn, Joo Hun Lee, Seungju Yang, Seung Cheol Lee, Hyunjoon Kong, and Hyun Jung Chung**

Drug-resistant microorganisms cause serious problems in human healthcare, leading to the persistence in infections and poor treatment outcomes from conventional therapy. In this study, a gene-targeting strategy using microbubble-controlled nanoparticles is introduced that can effectively eliminate biofilms of methicillin-resistant *Staphylococcus aureus* (MRSA) in vivo. Biofilm-targeting nanoparticles (BTN) capable of delivering oligonucleotides are developed that effectively remove biofilm-associated bacteria upon controlled delivery with diatom-based microbubblers (MB). The activity of BTN in silencing key bacterial genes related to MRSA biofilm formation (*icaA*), bacterial growth (*ftsZ*), and antimicrobial resistance (*mecA*), as well as their multi-targeting ability in vitro is validated. The integration of BTN with MB is next examined, resulting in synergistic effects in biofilm removal and antimicrobial activity in an ex vivo porcine skin model. The therapeutic efficacy is further investigated in vivo in a mouse wound model infected with MRSA biofilm, which showed that MB-controlled BTN delivery substantially reduced bacterial load and led to the effective elimination of the biofilm. This study underscores the potential of the gene silencing platform with physical enhancement as a promising strategy to combat problems related to biofilms and antibiotic resistance.

1. Introduction

The emergence and spread of infections with multidrug-resistant microbes pose a serious threat to human healthcare, expected to cause mortality of 40 million deaths and healthcare costs of up to $1.6 trillion each year by 2050.[1,2] It has been reported that over 70% of hospital-acquired infections in humans are caused by multidrug-resistant bacteria, such as *S. aureus, K. pneumoniae, E. coli*, and *A. baumannii*.[3] Particularly, *S. aureus* is known as the most prevalent among the Gram-positive bacterial pathogens, which is normally a part of the human flora of the skin, nose, mouth, eyes, and stomach.[4] In 2020, ≈80 000 cases in the United States were reported as infections with MRSA, and the number has increased by 3% annually.[5] However, hurdles in novel antibacterial discovery have led to limited treatment options in the clinic, requiring alternative strategies.[6]

Further complicating treatment, microorganisms including bacteria easily form biofilm structures that limit the penetration of bioactive molecules and host cells, resulting in persistent infection and poor responses to conventional therapies.[7] Biofilms consist of microbial communities encased in a self-produced extracellular polymeric matrix (EPS), which provides a physical barrier against antimicrobial agents and host immune responses.[8] It is estimated that biofilms are associated with ≈80% of all bacterial infections in humans, involving chronic wounds, biomedical implants and devices, transplantation, and complications from respiratory diseases or chronic disorders.[9] Biofilm resilience arises from multiple factors, including reduced permeability, horizontal transfer of resistance genes, and persistent bacteria

J. Y. Chung, S. Yang, S. C. Lee, H. J. Chung
Department of Biological Sciences
Korea Advanced Institute of Science and Technology
Daejeon 34141, Republic of Korea
E-mail: hyunjc@kaist.ac.kr

Y. Ahn, J. H. Lee, H. Kong
Department of Chemical and Biomolecular Engineering
University of Illinois at Urbana- Champaign
Urbana, IL 61801, USA
E-mail: hjkong06@illinois.edu

Y. Ahn, H. Kong
Chan Zuckerberg Biohub Chicago
Chicago, IL 60642, USA

H. Kong
Scott H. Fisher Multi-Cellular Engineered Living Systems Theme
Carl R. Woese Institute for Genomic Biology
University of Illinois at Urbana-Champaign
Urbana, IL 61801, USA

The ORCID identification number(s) for the author(s) of this article can be found under https://doi.org/10.1002/adfm.202508291

DOI: 10.1002/adfm.202508291

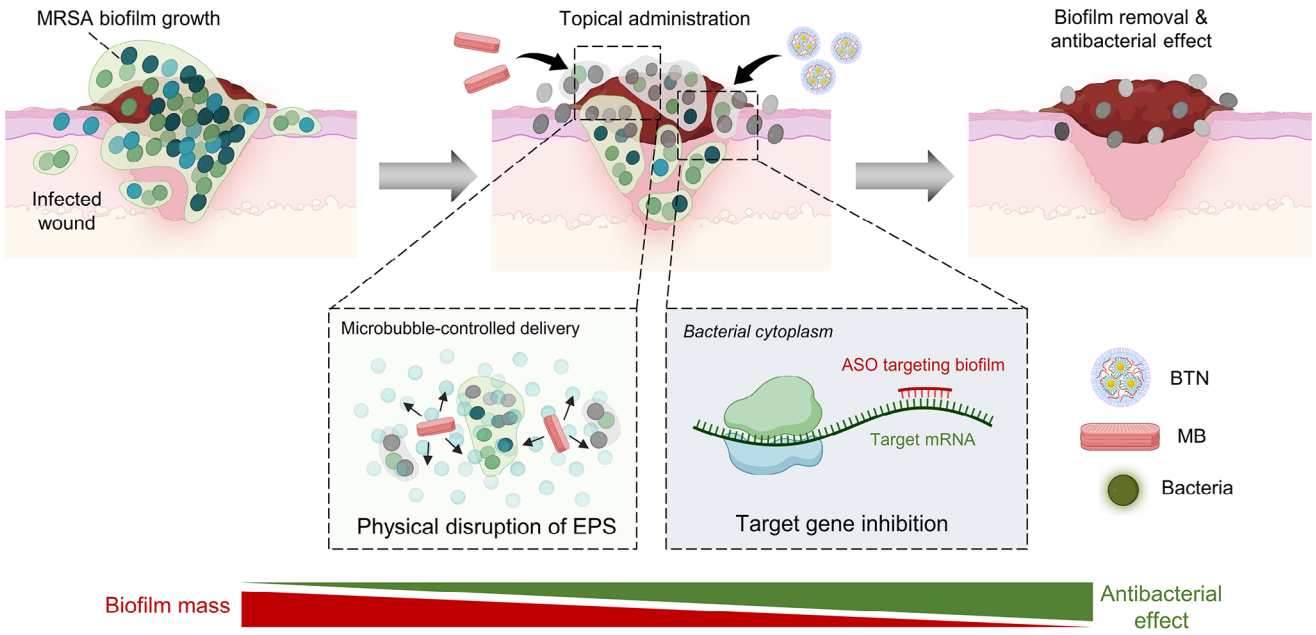

Figure 1. Effective biofilm treatment based on biofilm-targeting nanoparticles controlled with a microbubbler system. Schematic illustrating the treatment of BTN with controlled delivery by MB, allowing the effective permeation of ASOs targeting bacterial genes to biofilms infecting skin wounds. Silencing of bacterial genes related to biofilm growth, proliferation, and resistance results in effective biofilm removal and antibacterial efficacy in vivo.

against antibiotics.[10] The robust nature and resilience of bacterial biofilms lead to poor treatment outcomes, increasing healthcare costs and raising the global burden of antibiotic resistance.

Previous efforts to enhance bioactive molecule transport into biofilms have employed physical debridement or nanoparticle-based drug carriers.[11] Physical methods, such as ultrasound[12] and electric fields,[13] have demonstrated limited efficacy due to incomplete biofilm removal and potential damage to host tissues. Delivery vehicles like liposomes and polyplexes often raise concerns regarding toxicity, primarily because of nonspecific targeting and the potential risk of inducing antimicrobial resistance.[14] Alternative strategies based on gene targeting have been proposed, however were only demonstrated in vitro in cultures of planktonic bacteria.[15]

Here, we propose a gene-targeting strategy using biofilm-targeting nanoparticles (BTN) controlled with a microbubbler (MB) system, aiming to effectively treat bacterial biofilms in vivo (**Figure 1**). We developed BTN-delivering antisense oligonucleotides (ASOs) designed to silence bacterial genes associated with biofilm formation, growth, and antibiotic resistance. Our results demonstrated that BTN substantially inhibited planktonic MRSA activity, effectively preventing biofilm reformation. Treatment of BTN with MB propelled by oxygen microbubbles,[16] results in a dramatic enhancement in biofilm removal in vitro and in an ex vivo porcine skin model. Furthermore, we examine a mouse skin wound model infected with MRSA biofilm, where treatment of BTN with MB leads to effective elimination of the biofilm and accelerated wound healing efficacy. The current study not only demonstrates the potential of the gene targeting approach as an alternative strategy for antimicrobial treatment, but also provides an integrated platform to maximize therapeutic efficacy for practical use.

2. Results and Discussion

2.1. Development of BTN Targeting Bacterial Biofilm

We established a nanoplatform that can effectively deliver ASO-targeting genes related to biofilm formation into bacteria. Three candidate genes were selected as the target for ASO, which included *icaA*,[17] *ftsZ*,[18] and *mecA*,[19] which are related to biofilm formation, bacterial proliferation, and antibiotic resistance, respectively (**Figure 2a**), We constructed biofilm-targeting nanoparticles (BTNs) using gold nanoparticles (GNP, 5 nm core) modified with a cationic polymer (pGNP), that were subsequently loaded with ASOs, and further coated with chitosan (CS) (Figure 2a). Dynamic light scattering (DLS) analysis revealed that the nanoparticle (NP) size before loading with ASO was 56.9 nm, which increased to 74.8 nm upon ASO loading, and then to 143.8 nm following the addition of CS (Figure S1a, Supporting Information). The zeta potential appeared to be +1.27 mV, which decreased to –11.3 mV upon ASO loading and then increased to +37.6 mV after adding CS (Figure S1b, Supporting Information). The size and zeta potential did not significantly change when the ASO concentration was varied between 10 and 100 μM. Transmission electron microscopy (TEM) showed that BTN consisted of an organic matrix including multiple GNPs, with a mean diameter of ≈150 nm which were uniform upon complexation by electrostatic interactions between the cationic polymer-modified NP, ASO, and CS (Figure S2, Supporting Information). The loading efficiency of ASO in BTN was ≈98.7% when the initial ASO concentration was 0.5 μM, while that of the unmodified NPs was 15.9% (Figure S3, Supporting Information). The loading efficiency decreased to 35.2% when the initial ASO concentration was increased to 100 μM.

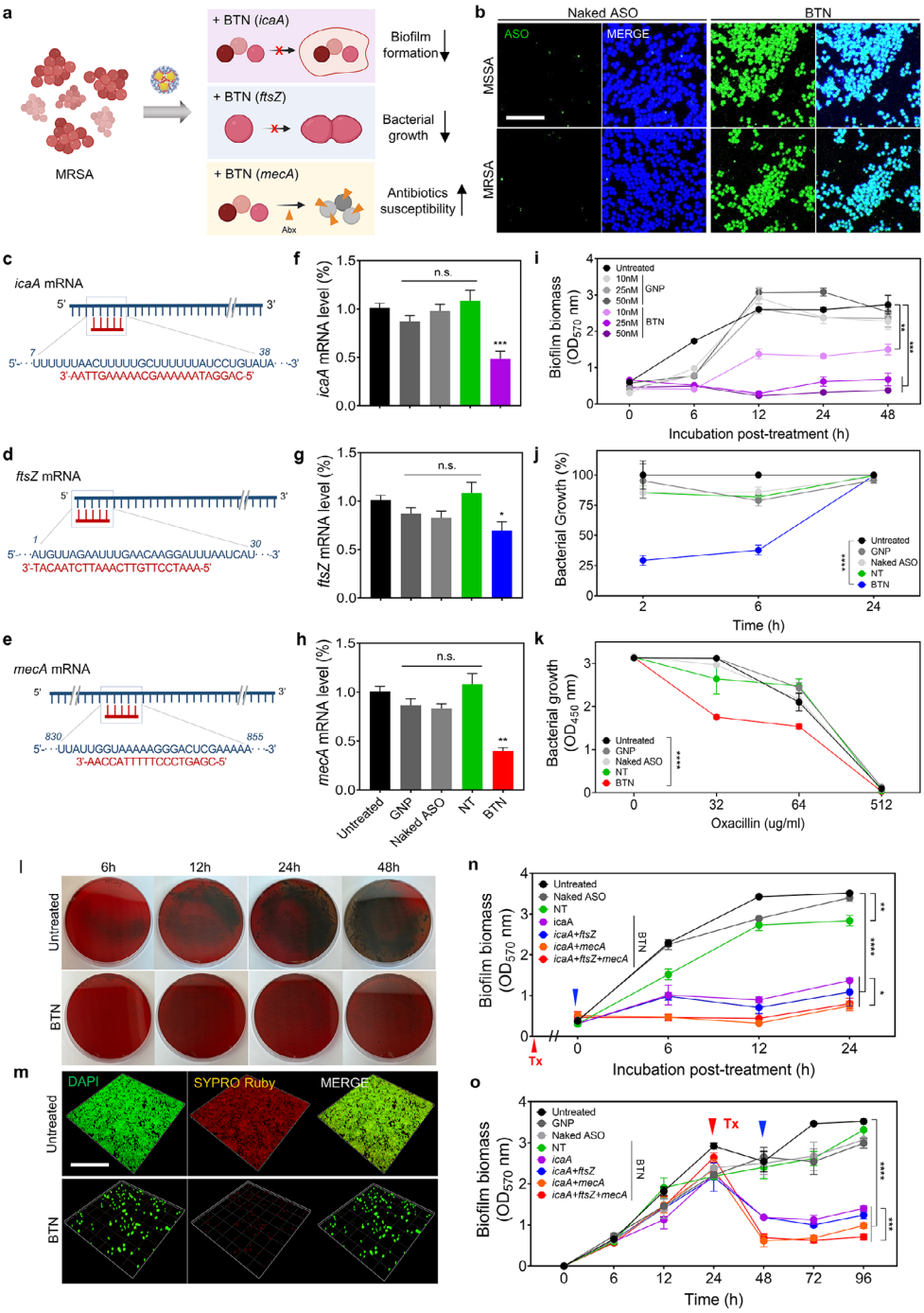

Figure 2. Effect of BTN on MRSA biofilm in vitro. a) Schematic showing the effect of BTN targeting genes *icaA*, *ftsZ*, or *mecA* on MRSA biofilm in inhibiting biofilm formation, reducing bacterial growth, and restoring antibiotic susceptibility. b) Bacterial uptake of ASO via BTN in MSSA (top) and MRSA (bottom), compared with naked ASO as the control. Green, FAM-labeled ASO; blue, nuclei stained with DAPI. Scale bar, 20 µm. c–e) Sequences of ASOs targeting *icaA* (c), *ftsZ* (d), and *mecA* (e) genes specific to MRSA. f–h) mRNA expression levels of *icaA* (f), *ftsZ* (g), and *mecA* (h) in MRSA treated with BTN (50 nM) or control formulations GNP (50 nM), naked ASO (50 µM), or BTN including non-target ASO (NT) (50 nM) for 2 h (n = 3–9). Target mRNA expression levels were normalized to 16S rRNA levels. i) Measurement of MRSA biofilm growth upon treating BTN targeting *icaA* (n = 2). j) Bacterial growth after BTN treatment in MRSA biofilm (n = 2). k) Antibiotic susceptibility assessed by treating BTN to MRSA biofilm in the presence of oxacillin (n = 2). l,m) Visualization of EPS in MRSA biofilms treated with BTN targeting icaA by (l) Congo red agar assay and (m) SYPRO Ruby staining. Green, DAPI; red, SYPRO Ruby. Scale bar, 50 µm. n,o) Effect of multi-targeting BTN including combinations of ASOs on MRSA biofilms before (n) and after (o) maturation in the presence of 32 µg mL^{-1} oxacillin (n = 2–3). Red and blue arrows indicate time points of BTN treatment and media, respectively. Data represent mean ± s.e.m. ($^{****}P < 0.0001$, $^{***}P < 0.001$, $^{**}P < 0.01$, $^{*}P < 0.05$; Two-way ANOVA). Data represented from two (f,g,h,o) or three (i,j,k,n) independent sets of experiments.

We next examined the internalization efficiency of BTN into bacterial cells in vitro. When BTN was treated to methicillin-sensitive *S. aureus* (MSSA) and methicillin-resistant *S. aureus* (MRSA), substantial uptake of ASO was shown in the bacterial cytoplasm, whereas naked ASO exhibited minimal internalization (Figure 2b). The efficient uptake of BTN was also observed across different bacterial species, such as *S. epidermidis*, *B. subtilis*, *E. coli*, and *P. aeruginosa* (Figure S4, Supporting Information). The non-specific delivery of BTN into mammalian cells was assessed by treating on NIH-3T3 cells, which exhibited minimal internalization compared to the controls (Figure S5, Supporting Information). Viability measurements upon treating BTN to NIH-3T3 cells for up to 72 h demonstrated that BTN did not induce significant cytotoxicity (Figure S6, Supporting Information). In sum, these findings suggest that BTN can efficiently deliver ASO to bacteria, while non-specific uptake into mammalian cells and off-target effects are minimized, thereby demonstrating a safe and potent in vivo delivery platform for targeting bacteria and their biofilms.

2.2. Examination of Antibiofilm Activity with BTN In Vitro

We investigated whether BTN-delivering ASOs could silence the target genes, leading to an antibiofilm effect in vitro. Here, we selected three target genes in MRSA, *icaA* which encodes the enzyme for synthesis of EPS,[17] *ftsZ* which is essential in bacterial growth,[18] and *mecA* which is the resistance gene of MRSA[19] (Figure 2c–e). Quantification of target mRNA expression levels revealed that treatment with BTN delivering ASO targeting either *icaA*, *ftsZ*, or *mecA* to MRSA resulted in a significant reduction in expression of 51.3%, 30.6%, and 59.8%, respectively (Figure 2f–h). The gene silencing effect was also shown for BTN delivering ASOs targeting *icaA* and *ftsZ* to MSSA (Figure S7a,b, Supporting Information). This demonstrates that mRNA degradation occurs substantially with the designed ASOs, which can be the main mechanism that induces target inhibition leading to the antibiofilm effect.[20]

We next examined the antibiofilm activity when treating BTN to bacterial biofilms. Notably, BTN loaded with *icaA*, a key regulatory gene in biofilm EPS formation, exhibited a potent and prolonged effect in inhibition of biofilm growth (88.8%) for ≈48 h, while the GNP controls did not (Figure 2i). Moreover, increasing the treatment dosage from 10 to 50 nM resulted in significant enhancements in the antibiofilm effect, from 40.4% to 88.8% compared to the GNP controls. BTN delivering ASO targeting *ftsZ*, an essential gene for bacterial cell division and proliferation, also exhibited significant suppression of MRSA biofilm growth (70.7%–62.3%) for up to 6 h (Figure 2j). However, although BTN targeting *ftsZ* showed a substantial effect on MRSA biofilms compared to the controls GNP, naked ASO, and BTN including non-target ASO (NT), the effect was not sustained enough, showing recovery of bacterial growth at 24 h. This can cause limitations in biofilm removal since a substantial portion of the bacterial community is persisting and continues to produce EPS, which can even strengthen the biofilm structure. On the other hand, treating BTN targeting *ftsZ* to MSSA biofilm showed stronger effects, possibly due to the weaker persistency in bacterial growth compared to MRSA[21] (Figure S8, Supporting Information). It was shown that BTN prepared with CS coating was superior to those prepared with polyethyleneimine (PEI) coating, a strong cationic polymer known for its potent transfection efficiency (Figure S9a,b, Supporting Information). BTN targeting the resistance gene *mecA* and subsequent silencing could lead to restoration of antibiotic susceptibility in MRSA, leading to up to 43.5% suppression of bacterial growth (Figure 2k). These results demonstrate the feasibility of BTN in the delivery of single ASOs to bacterial cells of MRSA and MSSA, leading to gene silencing and substantial suppression of biofilm growth.

Among the three target genes, *icaA* was found to be the most effective target for biofilm treatment. The effect of BTN targeting *icaA* was further characterized by Congo Red staining which allows the visualization of EPS production. Results showed that BTN treatment inhibited EPS formation as evidenced by the absence of black aggregates over time (Figure 2l). Confocal microscopy after staining with SYPRO Ruby also demonstrated that the majority of the biofilm was eradicated, with a dramatic reduction in EPS content in the MRSA biofilm (Figure 2m). Similar results were shown when treating BTN to MSSA biofilm (Figure S10, Supporting Information).

We further investigated whether multiple ASO delivery using BTN could lead to combinatorial effects in inhibiting biofilm growth. We performed the experiment by varying the incubation time after treatment with BTN delivering different ASO combinations. At an early stage of biofilm formation, BTN treatment could effectively inhibit biofilm formation, with a stronger effect when delivering multiple ASOs compared to a single ASO (Figure 2n). That is, delivering a combination of ASOs targeting *icaA*, *ftsZ*, and *mecA* resulted in a significant enhancement in biofilm inhibition (77.1%) compared to single ASO delivery (62.8%), demonstrating the synergistic effect of silencing two or more genes. In a matured biofilm model, which comprises high EPS content and resistance to antibiofilm agents,[22] BTN treatment resulted in significant suppression of biofilm growth starting from 48 h and lasted until 96 h (72.8%–80.0%), with triple ASO delivery (Figure 2o). This effect was superior compared to single ASO delivery, which resulted in 14.3% inhibition. We examined the immunogenicity of BTN by treating RAW 264.7 cells, which showed that no significant cytokine release occurred, whereas LPS treatment induced marked upregulation of TNF-α, IFN-β, and ISG15 expression by 20.3-fold, 22.2-fold, and 9.2-fold, respectively (Figure S11, Supporting Information). In sum, multiple gene silencing related to EPS formation, bacterial growth, and antibiotic resistance by BTN exerted a synergistic effect on biofilm inhibition, providing a potent strategy for the effective elimination of biofilm formation and antibacterial activity.

2.3. Effect of BTN Controlled with MB in an Ex Vivo Porcine Skin Model

The major challenge in the effective removal of bacterial biofilms lies in the low penetration of the agent deep into the core of the biofilm structure adhering to the host skin epithelium.[23] The EPS component of the biofilm creates a formidable barrier that hinders antibiotics from reaching the bacteria. Furthermore, prolonged antibiotic exposure predominantly affects the bacteria close to the surface, allowing bacteria residing in deeper

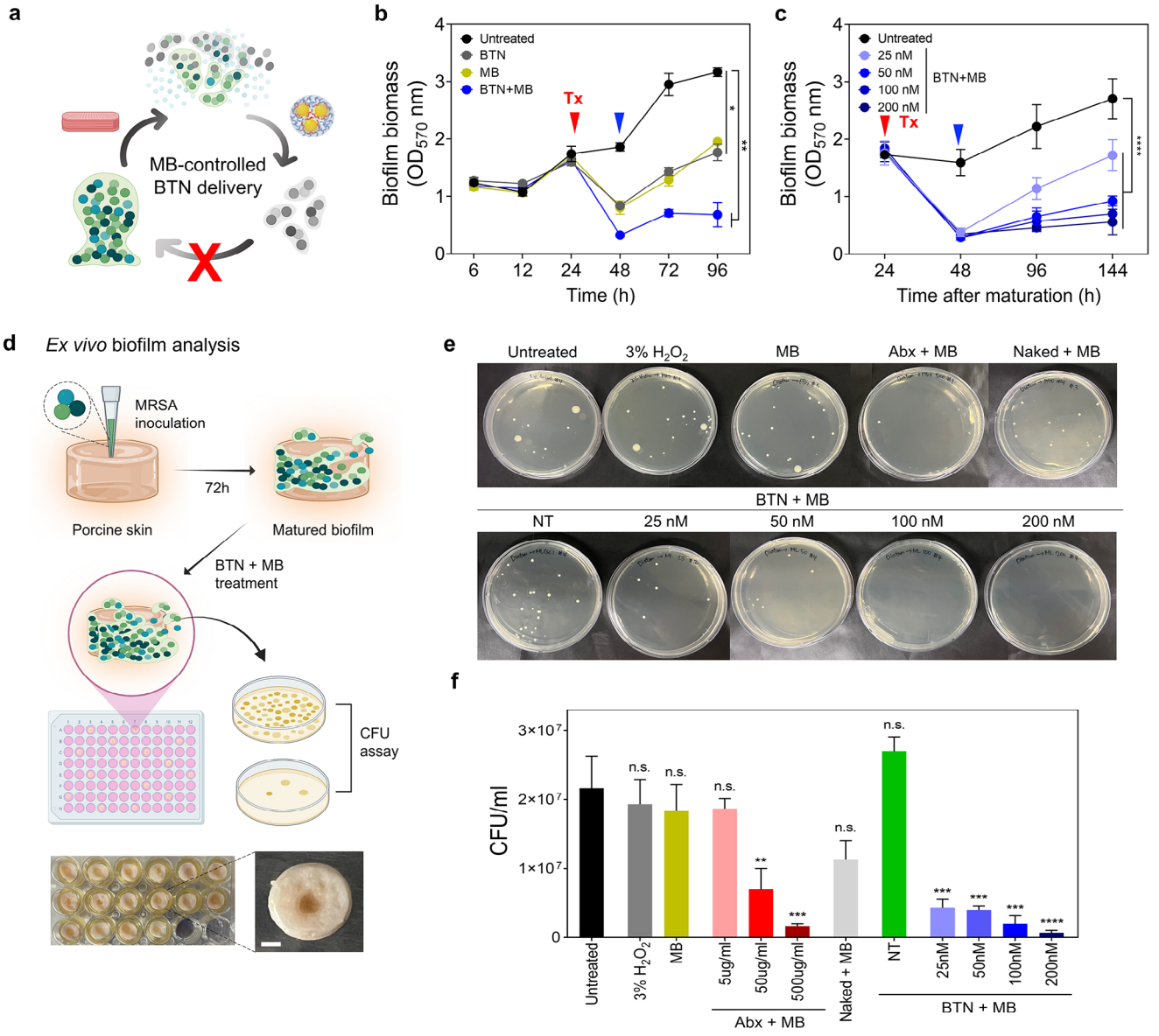

Figure 3. Effect on MRSA biofilm removal by BTN controlled with MB in vitro and ex vivo in porcine skin model. a) Overview of the synergistic effect of BTN treatment with MB on biofilm removal. b,c) Biofilm growth upon treatment of BTN targeting *icaA* combined with MB (BTN+MB) on mature MRSA biofilms. b) Comparison of BTN+MB with MB alone (MB) ($n = 3$). c) Treatment of BTN+MB at various doses ($n = 3$). Red arrows indicate the time points of treatment. d) Schematic on the ex vivo porcine skin model and procedure of measuring biofilm growth. Scale bar, 3 mm. e) Gross images and f) quantification of bacteria (CFU ml^{-1}) isolated from porcine skin explants treated with BTN targeting *icaA* along with MB (25–200 nM) or control formulations ($n = 3$). Data represent mean ± s.e.m. ($^{****}P < 0.0001$, $^{***}P < 0.001$, $^{**}P < 0.01$, $^{*}P < 0.05$; Two-way ANOVA). Data represented from three (b,c) or two (f) independent sets of experiments.

locations to develop resistance. This leads to the high recurrence rate of biofilm infections, suggesting that there is an urgent need to develop effective treatment strategies while minimizing the chance of antibiotic resistance over long-term applications. To address these challenges, we used a synergistic approach by combining BTN with a microbubbling method[24] for physical disruption of the biofilm (**Figure 3a**). MB consists of diatoms coated with chitosan (CS) and MnO_2 which can generate microbubbles upon reaction with H_2O_2 powerful enough to physically disrupt the biofilm structure. This would enhance the diffusion of substances including BTN through the biofilm by the increased permeability. Therefore, the combination of BTN with MB was expected to induce synergistic effects in antibacterial activity and biofilm elimination.

We first evaluated the combination treatment of BTN targeting the *icaA* gene and MB on mature MRSA biofilms. Individually, BTN and MB treatments resulted in 38.2% and 44.3% inhibition of biofilm formation, respectively, after 96 h. However, the combined treatment of BTN and MB achieved an inhibition rate of 78.5%, which was significantly higher than MB or BTN

treatment alone, with inhibition rates of 40.6% and 46.8%, respectively (Figure 3b). This finding highlights the potential of integrating physical and chemical approaches for sustained treatment and preventing the recurrence of biofilms. Furthermore, the efficacy of the antibiofilm effect exhibited a dose-dependent increase from 25 to 200 nM, with 37.0% inhibition observed at 25 nM and 81.5% inhibition at 200 nM. Higher concentrations of BTN leading to maximal antibiofilm activity, which persisted up to 120 h post-treatment (Figure 3c). Given the increased complexity and adhesion properties of biofilms in real tissues compared to in vitro cultured suspensions of bacteria, we employed a porcine skin infection model that better resembles real skin tissues. MRSA was inoculated on the pig skin and allowed to grow for 72 h for maturation of the biofilm (Figure 3d). Following this, the infected tissue was treated with the combination of BTN and MB, or the controls, and bacterial colonies were counted (Figure 3e,f). Notably, the combination of BTN and MB resulted in the most significant biofilm inhibition (>32-fold reduction versus untreated), which was comparable to when treated with combinations of MB and conventional antibiotics at high-dose (>13.5-fold reduction versus untreated). These results provide strong evidence for the potential of the combinatorial approach with BTN and MB, suggesting its applicability as an effective platform for treating bacterial biofilm infections in vivo.

2.4. In Vivo Efficacy in an MRSA Biofilm Model in Mice Wounds

To evaluate the in vivo antibacterial efficacy of BTN with MB, we employed a wound infection model with MRSA biofilm in mice (**Figure 4a**). Full-thickness wounds were created on the mice skin followed by inoculation with MRSA and allowing the biofilm to form for three days. We then administered either BTN delivering ASO targeting *icaA* alone or in combination with MB and monitored the wound healing process for 14 days. Treatment of BTN combined with MB exhibited strong antibiofilm efficacy with 23 000-fold reduction in bacterial colonies on day 6, while BTN alone also showed a significant effect with 180-fold reduction compared to the control (Figure 4b). Notably, the combination of BTN with MB completely eradicated the biofilm at 10 days (≈0 colonies detected), while BTN alone showed moderate efficacy with $>10^4$-fold reduction of bacterial colonies compared to the control (Figure 4c). Throughout the experiment, the control group showed substantial bacterial and biofilm growth (≈4.9×10^5 CFU ml^{-1}), which persisted over the observed time period. The combination of BTN and MB also resulted in accelerated wound closure rates compared to the control or BTN alone, which should be associated with strong antibacterial activity. After 14 days, the wound closure rates were 79.3% for the control group, 89.0% for the BTN group, and 93.6% for the BTN+MB group (Figure 4d). Histological analysis revealed that the control group exhibited severe inflammatory responses, significant epidermal damage, and extensive tissue degeneration, with indications of necrosis and fibrosis (Figure 4e). In contrast, the combination of BTN with MB facilitated well-organized epidermal regeneration, markedly reduced inflammatory cell infiltration, and restored structural features in the skin tissue such as diminished adhesion and the presence of hair follicles. Although BTN alone promoted some extent of tissue regeneration, residual tissue damage was observed. Immunohistochemistry analysis showed that the combined treatment of BTN with MB led to a gradual reduction in pro-inflammatory factors such as IL-6 and CD86 indicating M1 macrophages (Figure 4f), while anti-inflammatory factors including IL-10 and CD206 resembling M2 macrophages progressively increased (Figure 4g). Quantification of the pro-inflammatory factors IL-6 and CD86 (Figure 4h,i), as well as the anti-inflammatory factors IL-10 and CD206 (Figure 4j,k) further confirmed the superior effect of BTN with MB, compared to the moderate effect of BTN alone. Specifically, the pro-inflammatory markers IL-6 and M1 macrophages decreased by 54% and 82.5%, respectively, while the anti-inflammatory markers IL-10 and M2 macrophages increased by 243% and 226%, respectively. These results demonstrate that the strategy of combination treatment of BTN with MB effectively mitigates biofilm growth, relieving the infection and promoting tissue recovery as well as anti-inflammatory responses.

Overall, the current strategy of combining physical disruption with the gene-targeting nanoplatform can induce potent antibacterial effects that diminish biofilm growth and result in facilitated wound recovery. This highlights the potential of the method for treating biofilms related to post-surgical infections, medical implants and devices, and wound infections. Furthermore, the gene targeting approach using the BTN platform presents a promising strategy that can overcome the emerging problems of antibiotic resistance.

3. Conclusion

Biofilm-associated infections remain a major clinical challenge due to their resistance to conventional treatments and high recurrence rates. In this study, we developed a dual strategy based on BTN controlled with MB for effective biofilm removal and antibacterial effects. Microbubbles generated by MB effectively dismantled the structure of the biofilm and improved BTN penetration, while BTN selectively silenced key bacterial genes related to biofilm formation, bacterial growth, and antibiotic resistance. This synergistic approach demonstrated strong antibiofilm efficacy in both ex vivo and in vivo models, which were associated with effective bacterial clearance, accelerated wound healing, and reduced inflammation. By integrating physical disruption with a gene-targeting platform, the current study presents a promising solution to combat biofilm-related infections and antibiotic resistance. Based on the current study which validated the platform in cutaneous models, further efficacy studies in biofilms infecting biomedical implants (e.g., bone prostheses, heart pacemakers, stents) and devices (e.g., catheters, ports, ventilators) should be performed to evaluate the potential for practical applications in the clinic.

4. Experimental Section

Materials: GNPs (5 nm) functionalized with N-hydroxysuccinimide (NHS) ester (≈1 NHS group per nm^2) were obtained from Cytodiagnostics. BPEI (Mw 25 kDa) and chitosan oligosaccharides (CS) (Mw 5 kDa) were purchased from Sigma–Aldrich. Oligonucleotides used as ASOs and primers were supplied by Macrogen.

Fabrication of BTN: GNPs (1.1×10^{13} particles ml^{-1} in 1 mM NaCl) were reacted with 1.0 μg ml^{-1} BPEI and incubated at room temperature

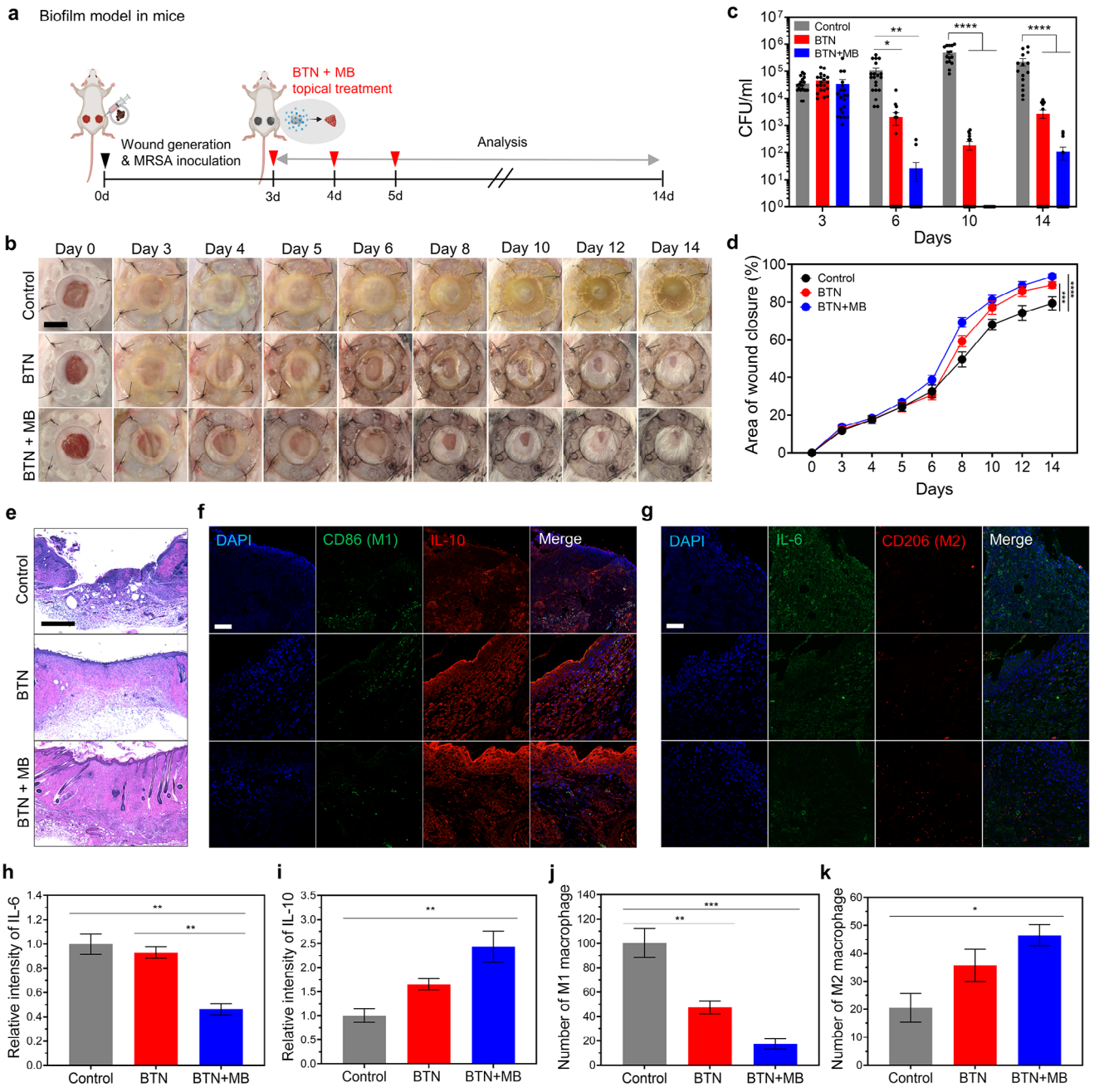

Figure 4. In vivo efficacy of MRSA biofilm removal in a mouse skin infection model. a) Scheme showing the timeline of in vivo evaluation of antibiofilm efficacy in MRSA-infected skin wounds of mice. BTN targeting *icaA* along with MB (BTN+MB) was treated once per day for three consecutive days (red arrows). b) Representative images of wounds after treatment with BTN+MB or MB as the control. Scale bar = 5 mm. c) Quantification of bacterial load (CFU mL^{-1}) in infected wounds following treatment with BTN+MB ($n = 15$–20). d) Area of wound regeneration measured during the time period ($n = 5$). e) Histological analysis of skin tissues harvested on day 14, stained with hematoxylin and eosin (H&E). Scale bar = 500 µm. f,g) Immunohistochemical (IHC) staining of pro-inflammatory and anti-inflammatory markers in skin tissues harvested on day 14. Representative IHC images after staining for (f) M1 macrophages (green) and IL-10 (red), and (g) M2 macrophages (red) and IL-6 (green). Scale bar = 50 µm. h–k) Quantification of fluorescence for (h) IL-6, (i) IL-10, (j) M1 macrophages, and (k) M2 macrophages from images shown in f and g ($n = 3$–4). Data represent mean ± s.e.m. ($^{***}P < 0.001$, $^{**}P < 0.01$, $^{*}P < 0.05$; One-way ANOVA).

(RT) with gentle stirring for 1 h. Unbound BPEI was removed by three washes with centrifugal filters (Amicon Ultracel, MWCO 100 kDa), and the purified GNPs were resuspended in 10 mM NaCl. The BPEI-conjugated GNPs were then incubated with ASO (10–100 μM) at RT under gentle agitation for 30 min. After two additional washes using centrifugal filters, the GNP/ASO complexes were resuspended in 10 mM NaCl and subsequently mixed with 2.0 μg ml^{-1} CS, followed by incubation at RT with gentle stirring for 1 h. The final complexes were washed again via centrifugal filtration and resuspended in 10 mM NaCl to obtain BTN.

Fabrication of MB: The diatom microbubblers (MB) were fabricated by coating MnO_2 nanosheets on the pores of hollow cylindrical diatoms. First, 400 mg of diatoms (Diatomaceous Earth-food grade, amorphous silica from freshwater type) were washed with deionized water (DW) and collected using a centrifuge (Eppendorf) at 1000 rpm for 3 min. Then, 20 mL of fresh DW was added, resulting in a diatom slurry, and 30 mL of low-molecular-weight chitosan solution (Tidal Grow, Tidal Vision) was added to the diatom slurry. The chitosan-mixed diatom slurry was stirred for 30 min using a stirrer (Thermo Fisher) at 500 rpm. Then, the particles were collected by centrifugation at 4000 rpm for 8 min and washed with DW three times. The chitosan-coated diatom particles were dried in a lyophilizer (Labconco) for 12 h and collected as dry powder. For the formation of MnO_2 nanosheets on the chitosan-coated diatoms, 20 mL of 0.1 M $KMnO_4$ (Sigma–Aldrich) was added to 200 mg of chitosan-coated diatoms and stirred at 500 rpm for 4 h. Then, the particles were collected by centrifugation at 1000 rpm for 3 min and washed with DW three times. The resulting MnO_2-chitosan-coated diatoms, denoted as diatom microbubblers (MB), were dried in a lyophilizer for 12 h and collected as dry powder.

Characterizations of BTN: Dynamic light scattering (DLS) and zeta potential measurements were conducted using ELSZ-2000 (Otsuka). For transmission electron microscopy (TEM), samples were stained with a 0.5% ruthenium tetroxide solution (Sigma–Aldrich), applied to a 300-mesh carbon grid (Electron Microscopy Sciences, Inc.), and analyzed using a Tecnai G2 Spirit TWIN (Thermo Fisher Scientific). Loading efficiency (%) was calculated as the difference between the initial and remaining amounts of ASO, measured using 5′-FAM-ASO, divided by the initial ASO amount, as expressed in the following equation:

$$\text{Loading efficiency } (\%) = \frac{(\text{Initial amount of ASO} - \text{filtrate amount of ASO})}{(\text{Initial amount of ASO})} \times 100 \quad (1)$$

Bacterial Strains and Culture: MRSA strain CCARM 3798 was obtained from the Culture Collection of Antimicrobial Resistant Microbes. Bacterial strains of MSSA KCTC 3881, *S. epidermidis* KCTC 1917, *B. subtilis* KCTC 1021, *E. coli* KCTC 1682, and *P. aeruginosa* KCTC 2004 were provided by the Korean Collection for Type Cultures. For bacterial culture, MRSA, MSSA, and *S. epidermidis* were cultured in Tryptic Soy Broth (TSB, Difco, BD), whereas *B. subtilis*, *E. coli*, and *P.aeruginosa* were grown in Luria–Bertani Broth (LB, Difco, BD). Bacteria were inoculated into the appropriate media and incubated in suspension at 37 °C with gentle agitation (180 rpm) using a shaking incubator (Jeiotech) for 12–16 h. Bacterial suspensions were transferred to fresh media and cultured for an additional 2–3 h. Bacterial growth was assessed by measuring the optical density at 600 nm (OD600) using NanoPhotometer (P330, Implen GmbH).

Cell Culture: NIH-3T3 mouse embryonic fibroblast cells and RAW264.7 mouse macrophage cells were sourced from the American Type Culture Collection (ATCC). Cells were cultured in Dulbecco's Modified Eagle Medium (DMEM) containing 25 mM 4-(2-hydroxyethyl)-1-piperazineethanesulfonic acid (HEPES) and L-glutamine (Thermo Fisher) supplemented with 10% heat-inactivated fetal bovine serum (FBS, Hyclone) and 1% penicillin/streptomycin (Thermo Fisher). Cell cultures were incubated at 37 °C in a CO_2 incubator (BB15, Thermo Fisher Scientific).

Uptake into Bacteria and Mammalian Cells: To evaluate bacterial uptake, 2×10^7 bacterial cells were inoculated onto microscopic 8-chamber slides (SPL Life Science) and treated with either BTN (50 nM) or naked ASO for 2 h, followed by two washes with PBS (pH 7.0). For mammalian cell experiments, 2×10^4 NIH-3T3 cells were seeded onto 8-chamber slides and incubated with BTN or control formulations for 6 h, then washed twice with PBS (pH 7.0). After treatment, both bacterial and mammalian cells were fixed with 4% paraformaldehyde, permeabilized with 0.1% Triton X-100, and washed twice with PBS. The cells were then mounted on microscopic slides using VectaShield with 4′,6-diamido-2-phenylindole (DAPI; Vector Laboratories) and visualized by confocal microscopy (LSM 980, Carl Zeiss). Image acquisition and analysis were performed using Zen Blue software (Carl Zeiss).

Gene Silencing Effect of BTN: MRSA and MSSA bacterial cells (4.8×10^7 CFU) were treated with BTN (50 nM) loaded with ASO targeting the *icaA*, *ftsZ*, or *mecA* genes at 37 °C with gentle stirring (180 rpm) for 2 h. Total RNA was extracted using TRIzol Reagent (Thermo Fisher Scientific), and cDNA was synthesized using the PrimeScript RT Reagent Kit (Takara Biotechnology Co., Ltd.) with random primers (Table S1, Supporting Information). Quantitative polymerase chain reaction (qPCR) was performed using PowerUp SYBR Green (Thermo Fisher Scientific) and specific primers for each target gene, on a QuantStudio 3 Real-Time PCR System (Thermo Fisher Scientific). The relative expression levels of *icaA*, *ftsZ*, and *mecA* were normalized to the expression of 16S rRNA.

Cytokine Expression Analysis in Myeloid Cells: RAW264.7 macrophage cells were starved in serum-free medium for 24 h prior to treatment. Cells were then treated with BTN (50 or 100 nM) or LPS (300 ng mL^{-1}) for 6 h at 37 °C. Total RNA was extracted using the RNAiso Plus reagent (Takara Bio Inc.), and cDNA was synthesized using the PrimeScript RT Reagent Kit (Takara Biotechnology Co., Ltd.) with random primers (Table S1, Supporting Information). Quantitative polymerase chain reaction (qPCR) was performed using PowerUp SYBR Green (Thermo Fisher Scientific) and specific primers for *TNF-α*, *IFN-β*, and *ISG15*, on a QuantStudio 3 Real-Time PCR System (Thermo Fisher Scientific). The relative mRNA expression levels of each cytokine were normalized to the expression of *GAPDH*.

In Vitro Analysis of Biofilm Growth: Biofilm growth was assessed by the crystal violet assay (Sigma–Aldrich). To evaluate on premature biofilms, bacteria (4.8×10^8 CFU) were cultured in 96-well plates and treated with BTN or control formulations (10–50 nM). For assessing the effect on mature biofilms, bacteria (4.8×10^8 CFU) were seeded in 96-well plates and incubated for 24 h, and planktonic bacteria were removed. Bacteria were then treated with BTN or control formulations (10–50 nM) followed by removing the planktonic bacteria, and the media was replaced with 1% glucose-containing media and incubated for another 6–48 h. To measure biofilm mass, planktonic bacteria were discarded followed by washing the biofilm twice with PBS (pH 7.4) to remove any non-adherent cells. The biofilm was stained with 0.1% crystal violet solution for 15 min at RT, washed, and added with 33% acetic acid. Absorbance was measured at 570 nm using a microplate reader (Infinite 200 PRO, Tecan, Ltd.). Biofilm growth was quantified by comparison of the absorbance of treated samples to that of controls, with a decrease in absorbance indicating reduced biofilm formation.

Antibacterial Effect: Bacterial growth of MRSA (4.8×10^7 CFU) was measured using the Microbial Viability Assay Kit-WST (Dojindo Molecular Technologies, Inc.) following the manufacturer's instructions. Bacteria were treated with BTN (50 nM) prepared with anti-mecA ASO (initial loading concentration: 100 μM) or control formulations for 24 h, followed by an additional 24 h incubation in fresh media containing 0, 32, 64, and 512 μg mL^{-1} of oxacillin. Then WST reagent was added, and bacteria were incubated at 37 °C for 1–2 h. Absorbance was measured at 450 nm using the Infinite 200 PRO (Tecan, Ltd.). For all in vitro experiments, an equivalent amount of ASO was treated in each experimental group for BTN and naked ASO.

Congo Red Assay: Congo Red agar plates were prepared by mixing 37 g of Brain Heart Infusion broth (BHI, Difco, BD), 50 g of sucrose (Sigma–Aldrich), and 10 g of agar in 1 L of distilled water. 0.8 g of Congo Red dye (Sigma–Aldrich) was dissolved in 10 mL of distilled water. The solution was sterilized separately by autoclaving for 15 min. After sterilization, the agar and Congo Red solution were mixed and poured into 90 mm petri dishes, and allowed the agar to solidify at RT. The prepared plates were stored at 4 °C until use. Bacteria (4.8×10^8 CFU) were cultured and treated with 50 nM of BTN for 24 h. Then, 100 μL of the bacterial suspen-

sion was spread evenly onto the surface of the prepared Congo Red agar plates using a sterile spreader and incubated at 37 °C for 24 h. Plates were visualized with EPS production indicated by a shift in color from red to black.

Confocal Microscopy of Biofilm: Bacterial cells (4.8×10^8 CFU) were cultured in 8-chamber slides and treated with BTN or control formulations at 37 °C for 24 h. Planktonic bacteria were removed, and the biofilm was washed twice with PBS (pH 7.4). SYPRO Ruby (1:1000 dilution, Thermo Fisher) was applied to the biofilm for 30 min at RT, followed by washing with PBS. The biofilm was then mounted with VectaShield including DAPI (Vector Laboratories) and observed using a confocal laser scanning microscope (LSM 980, Carl Zeiss). Biofilm structure and EPS production were analyzed using Zen Blue software (Carl Zeiss).

Ex Vivo Porcine Skin Model: Porcine skin explants were prepared based on adaptation from existing protocols. Fresh porcine skin, purchased from a local supplier, was first frozen overnight at −80 °C. The frozen skin was then cut into 12 mm diameter explants using a biopsy punch. A high-speed Dremel 300 drill with a cutting attachment was used to create a consistent central wound site of 3 mm diameter and 1.5 mm depth on each explant. The explants were immersed in PBS containing 0.0005 v/v% of Tween-80 (PBS-T; Sigma–Aldrich), and transferred to 70% ethanol solution in PBS-T for 30 min. After washing three times in PBS-T for 10 min and sterilization, the explants were placed at the center of a 24-well culture plate (SPL Life Science) and fixed using TSA agar (0.5% agar, oxacillin 500 µg mL^{-1}). MRSA (5×10^5 CFU was then inoculated onto the central wound site of each explant and incubated for 3 days. The bottom of each explant was fixed to a sterile lid of a 24-well plate using super glue. A rinse plate was prepared with PBS, and a test plate was prepared with PBS, 3 wt.% H_2O_2 solution, or 3 wt.% H_2O_2 solution with MB. The lid with the explants was quickly placed on the first rinse plate for 10 s to remove planktonic bacteria and then transferred to the test plate. After 10 min, the lid was moved to the second rinse plate for 10 s, treated with MB, followed by treatment with BTN (50–200 nM) for 24 h. After washing, the explants were transferred to a conical tube containing PBS-T, and sonicated at 20 W in an ice bath for 30 s. The bacterial suspension was serially diluted, plated onto TSA plates, and incubated overnight at 37 °C. Colonies were counted to obtain viable bacterial concentration (CFU mL^{-1}).

Full-Thickness Dermal Excisional Wound Model and Infection: All procedures were conducted in accordance with the guidelines for the care and use of laboratory animals and approved by the Institutional Animal Care and Use Committee (IACUC) of the University of Illinois at Urbana-Champaign (#23 153). Healthy 8-week-old male CD-1 mice (Charles River Laboratories) were anesthetized with 2% isoflurane in oxygen, and their backs were shaved. Full-thickness wounds with a diameter of 5 mm were created symmetrically on both sides of the back using a biopsy punch. To prevent wound closure by skin contraction, splints were secured around each wound using adhesive and sutures. For infected wound conditions, 20 µL of MRSA bacterial solution (10^6 CFU mL^{-1}) was applied topically to each wound. The wounds were then covered with a membrane filter to prevent leakage, and Tegaderm (3M) and bandages were wrapped around them, which were replaced daily.

Treatment of Infected Wounds: In order to evaluate the efficacy of the treatment method, the in vivo study included three treatment conditions: untreated (control), BTN (biofilm-targeting nanoparticles) only, and BTN with pre-treated MB (microbubblers). The treatment began on Day 3 post-wound infection for all groups. In the BTN-only group, the treatment was administered thrice on Days 3, 4, and 5. The BTN solution was absorbed into a disk-shaped sponge and applied to the infected site for 4 h, ensuring a steady and complete release of the BTN solution. The dose of BTN was standardized at 50 pmol per wound, with a treatment volume of 50 µL. For the BTN with a pre-treated MB condition, the MB treatment was administered only once on Day 3, and the BTN was administered on Days 3, 4, and 5 in the same manner as for the BTN-only condition.

Evaluation of In Vivo Efficacy: A standard colony-forming unit (CFU) measurement technique based on serial dilution is utilized to quantify the bacterial load on the wound. The infected wound area was swabbed using sterile swabs on Days 3, 6, 10, and 14. After swabbing, the samples were immediately suspended in phosphate-buffered saline (PBS). The suspension was diluted and plated onto tryptic soy agar (TSA) plates. These plates were incubated at 37 °C for 24 h, after which the colonies were counted manually. The bacterial load was calculated by multiplying the average number of colonies by the dilution factor, and the result was expressed as CFU per mL of the original sample.

To quantify the regenerated area, photographs of wounds were captured every 1–2 days for two weeks. The remaining wound area was measured using ImageJ software (National Institutes of Health) by manually selecting the wound boundary. The percentage of the regenerated area was calculated by dividing the regenerated area (initial wound area − remaining area) at each time point by the initial wound area, which was measured immediately after wound creation. All images were taken under standardized lighting conditions with a fixed camera distance to maintain consistency across measurements.

The harvested skin tissues on Day 14 were fixed in a 4% paraformaldehyde (PFA) solution to preserve tissue structure. Following fixation, the tissues were dehydrated through a graded ethanol series (70%, 95%, and 100%) and cleared in xylene before being embedded in paraffin. For embedding, tissues were oriented in molds filled with melted paraffin, which was allowed to solidify on a cold plate. Paraffin blocks were sectioned into 5 µm thickness slices using a microtome, and sections were mounted onto glass slides. After drying tissue slides, hematoxylin and eosin (H&E) staining was performed for tissue morphology analysis. Slides were deparaffinized in xylene, rehydrated through a graded ethanol series (100%, 95%, and 70%), and rinsed in DW. Sections were stained with hematoxylin for 3 min, rinsed in DW to allow stain development, briefly destained with acid alcohol, and counterstained with eosin for 30 s. Finally, slides were dehydrated through graded ethanol, cleared in xylene, and coverslipped with a mounting medium to preserve the stained sections for microscopic analysis.

In order to analyze inflammatory factors, the tissue slides were rehydrated through a graded ethanol series and rinsed in DW. The rehydrated tissues used the heat-induced epitope retrieval (HIER) method to expose antigenic sites, allowing antibodies to bind. In order to prepare the antigen retrieval buffer, a 0.1 M tri-sodium citrate dihydrate solution and 0.1 M citric acid monohydrate solution were prepared. The 11.5 mL of 0.1 M citric acid monohydrate solution was mixed with the 88.5 mL of 0.1 M tri-sodium citrate dihydrate solution to create 100 mL of 0.1 M citric acid-sodium citrate buffer at pH 6.0. This buffer was then diluted tenfold by combining the 0.1 M citric acid-sodium citrate buffer with DW to prepare a 0.01 M citric acid-sodium citrate buffer. Finally, the antigen retrieval buffer was prepared by adding 0.05% Tween-20 to the 0.01 M citric acid-sodium citrate buffer. The rehydrated tissue slide was immersed in the heat-induced epitope retrieval (HIER) buffer and processed in a pressure cooker for 10 min. After cooling down, the tissue slides were rinsed in PBS containing 0.05% Tween-20 twice (PBS-Tween), with each rinse lasting 2 min. The tissue slides were blocked with a blocking buffer containing 5 mg mL^{-1} of bovine serum albumin (BSA) for 30 min. Slides were incubated at 4 °C overnight with primary antibodies against IL-6 (1:100, MA5-45069, Invitrogen), CD86 (1:200, 14-0862-82, Invitrogen), IL-10 (1:100, MA5-42656, Invitrogen), and CD206 (1:200, MA5-16871, Invitrogen). Afterward, the tissue slides were incubated with secondary antibodies, anti-mouse AF488 (1:500, A-11001, Invitrogen) for IL-6, anti-rat AF488 (1:500, A-11006, Invitrogen) for CD86, anti-rabbit AF568 (1:500, A-11011, Invitrogen) for IL-10, and anti-rat AF568 (1:500, A78946, Invitrogen) for CD206, for 30 min at room temperature. The primary and secondary antibodies were diluted in a blocking buffer. Tissue slides were rinsed in PBS-Tween several times for 5 min and mounted with mounting medium (00-4959-52, Invitrogen), including DAPI. Immunofluorescence images were captured using a confocal microscope (LSM980, Zeiss).

Statistical Analysis: For all in vitro experiments, at least three independent sets of experiments were performed in triplicates for each group, unless otherwise stated. All statistical data were expressed as mean ± s.e.m., and analyses were carried out using GraphPad Prism v.9.0. Statistical significance was determined using one-way ANOVA, or two-way ANOVA to obtain the P value. $^{*}P \leq 0.05$, $^{**}P \leq 0.01$, $^{***}P \leq 0.001$, $^{****}P \leq 0.0001$ was considered statistically significant.

Supporting Information

Supporting Information is available from the Wiley Online Library or from the author.

Acknowledgements

J.Y.C. and Y.A. contributed equally to this work. This study was supported by grants from the National Research Foundation (RS-2024-00355464) and KAIST Grand Challenge Project (KC30), Republic of Korea; National Science Foundation (NSF-DMR 2004719) and National Institutes of Health (1R01AI160671-A1), USA.

Conflict of Interest

The authors declare no conflict of interest.

Data Availability Statement

The data that support the findings of this study are available from the corresponding author upon reasonable request.

Keywords

biofilm, gene silencing, microbubble, MRSA, nanoparticles

Received: April 2, 2025
Revised: April 29, 2025
Published online:

[1] a) E. M. Darby, E. Trampari, P. Siasat, M. S. Gaya, I. Alav, M. A. Webber, J. M. A. Blair, *Nat. Rev. Microbiol.* **2023**, *21*, 280; b) L. Hall-Stoodley, J. W. Costerton, P. Stoodley, *Nat. Rev. Microbiol.* **2004**, *2*, 95.

[2] M. Naghavi, S. E. Vollset, K. S. Ikuta, L. R. Swetschinski, A. P. Gray, E. E. Wool, D. M. Dekker, *Lancet* **2024**, *404*, 1199.

[3] A. Stacy, L. McNally, S. E. Darch, S. P. Brown, M. Whiteley, *Nat. Rev. Microbiol.* **2016**, *14*, 93.

[4] a) F. Gotz, *Mol. Microbiol.* **2002**, *43*, 1367; b) M. Brandwein, D. Steinberg, S. Meshner, *NPJ Biofilms Microbiomes* **2016**, *2*, 3.

[5] Z. Li, H. Zhuang, G. Wang, H. Wang, Y. Dong, *BMC Infect. Dis.* **2021**, *21*, 74.

[6] a) H. Zazo, C. I. Colino, J. M. Lanao, *J. Control Release* **2016**, *224*, 86; b) T. F. Mah, *Future Microbiol.* **2012**, *7*, 1061; c) P. J. Yeh, M. J. Hegreness, A. P. Aiden, R. Kishony, *Nat. Rev. Microbiol.* **2009**, *7*, 460.

[7] a) H. C. Flemming, J. Wingender, U. Szewzyk, P. Steinberg, S. A. Rice, S. Kjelleberg, *Nat. Rev. Microbiol.* **2016**, *14*, 563; b) H. Koo, R. N. Allan, R. P. Howlin, P. Stoodley, L. Hall-Stoodley, *Nat. Rev. Microbiol.* **2017**, *15*, 740; c) O. Ciofu, C. Moser, P. O. Jensen, N. Hoiby, *Nat. Rev. Microbiol.* **2022**, *20*, 621.

[8] a) H. C. Flemming, J. Wingender, *Nat. Rev. Microbiol.* **2010**, *8*, 623; b) L. Hobley, C. Harkins, C. E. MacPhee, N. R. Stanley-Wall, *FEMS Microbiol. Rev.* **2015**, *39*, 649.

[9] M. K. Yadav, J.-J. Song, B. P. Singh, J. E. Vidal, *New and Future Developments in Microbial Biotechnology and Bioengineering: Microbial Biofilms*, Elsevier, Amsterdam, Netherlands **2020**.

[10] a) A. Brauner, O. Fridman, O. Gefen, N. Q. Balaban, *Nat. Rev. Microbiol.* **2016**, *14*, 320; b) D. Davies, *Nat. Rev. Drug Discovery* **2003**, *2*, 114; c) H. Y. Liu, E. L. Prentice, M. A. Webber, *NPJ Antimicrob. Resist.* **2024**, *2*, 27.

[11] a) V. Choi, J. L. Rohn, P. Stoodley, D. Carugo, E. Stride, *Nat. Rev. Microbiol.* **2023**, *21*, 555; b) G. Hwang, A. J. Paula, E. E. Hunter, Y. Liu, A. Babeer, B. Karabucak, H. Koo, *Sci. Robot.* **2019**, *4*, aaw2388; c) J. Wang, G. Yu, Q. Fang, Y. Xu, J. Zhang, A. Hui, S. Xuan, K. C. Leung, *Adv. Healthcare Mater.* **2025**, https://doi.org/10.1002/adhm.202404208.

[12] a) W. Xia, Q. Cai, H. Wu, J. Li, Z. Zhou, C. Huang, B. Cheng, *Ultrason. Sonochem.* **2025**, *112*, 107100; b) Z. Hazan, J. Zumeris, H. Jacob, H. Raskin, G. Kratysh, M. Vishnia, N. Dror, T. Barliya, M. Mandel, G. Lavie, *Antimicrob. Agents Chemother.* **2006**, *50*, 4144; c) H. Yang, X. Zhan, L. Song, S. Cheng, R. Su, Y. Zhang, D. Guo, X. Lu, X. Xia, C. Shi, *Int. J. Food Microbiol.* **2023**, *391*, 110150.

[13] a) S. I. Khan, G. Blumrosen, D. Vecchio, A. Golberg, M. C. McCormack, M. L. Yarmush, M. R. Hamblin, W. G. Austen Jr., *Biotechnol. Bioeng.* **2016**, *113*, 643; b) K. G. Barki, A. Das, S. Dixith, P. D. Ghatak, S. Mathew-Steiner, E. Schwab, S. Khanna, D. J. Wozniak, S. Roy, C. K. Sen, *Ann. Surg.* **2019**, *269*, 756; c) R. B. Juncker, B. A. Lazazzera, F. Billi, *Microbiol. Spectr.* **2022**, *10*, 01949.

[14] a) M. A. Blaskovich, K. A. Hansford, M. S. Butler, S. Ramu, A. M. Kavanagh, A. M. Jarrad, M. A. Cooper, *Sci. Transl. Med.* **2022**, *14*, abj2381; b) A. De Breij, M. Riool, R. A. Cordfunke, N. Malanovic, L. de Boer, R. I. Koning, P. H. Nibbering, *Sci. Transl. Med.* **2018**, *10*, aan4044; c) X. Peng, J. Chen, Y. Gan, L. Yang, Y. Luo, C. Bu, X. Ding, *Sci. Adv.* **2024**, *10*, adk9754.

[15] M. J. Beha, J. S. Ryu, Y. S. Kim, H. J. Chung, *Mater. Sci. Eng. C* **2021**, *126*, 112167.

[16] a) Y. Seo, J. Leong, J. D. Park, Y. T. Hong, S. H. Chu, C. Park, D. H. Kim, Y. H. Deng, V. Dushnov, J. Soh, S. Rogers, Y. Y. Yang, H. Kong, *ACS Appl. Mater. Interfaces* **2018**, *10*, 35685; b) Y. H. Deng, T. Ricciardulli, J. Won, M. A. Wade, S. A. Rogers, S. A. Boppart, D. W. Flaherty, H. Kong, *Biomaterials* **2022**, *287*, 121610; c) H. Kim, E. H. Lee, S. W. Lee, Y. H. Deng, H. B. Kwon, Y. J. Lim, H. Kong, M. J. Kim, *BMC Oral Health* **2023**, *23*, 33.

[17] a) S. E. Cramton, C. Gerke, N. F. Schnell, W. W. Nichols, F. Götz, *Infect. Immun.* **1999**, *67*, 5427; b) J. P. O'Gara, *FEMS Microbiol. Lett.* **2007**, *270*, 179.

[18] a) P. Pradhan, W. Margolin, T. K. Beuria, *Front. Microbiol.* **2021**, *12*, 732796; b) N. Silber, C. L. Matos de Opitz, C. Mayer, P. Sass, *Future Microbiol.* **2020**, *15*, 801.

[19] a) Y. C. Ho, S. C. Chang, S. R. Lin, W. K. Wang, *J. Clin. Microbiol.* **2009**, *47*, 1443; b) T. Boonsiri, S. Watanabe, X. E. Tan, K. Thitiananpakorn, R. Narimatsu, K. Sasaki, R. Takenouchi, Y. Sato'o, Y. Aiba, K. Kiga, T. Sasahara, Y. Taki, F. Y. Li, Y. Zhang, A. H. Azam, T. Kawaguchi, L. Cui, *Sci. Rep.* **2020**, *10*, 16907.

[20] a) N. Angrish, G. Khare, *Med. Drug Discov.* **2023**, *20*, 100166; b) E. Ersoz, D. Demir-Dora, *Drug Dev. Res.* **2024**, *85*, 22187.

[21] J. Xiao, E. D. Goley, *Curr. Opin. Microbiol.* **2016**, *34*, 90.

[22] J. S. Temme, Z. Tan, M. Li, M. Yang, A. Wlodawer, X. Huang, J. S. Schneekloth Jr., J. C. Gildersleeve, *Cell Chem. Biol.* **2024**, *31*, 2096.

[23] S. L. Percival, C. Emanuel, K. F. Cutting, D. W. Williams, *Int. Wound J.* **2012**, *9*, 14.

[24] a) K. C. M. Le, A. T. Q. Tran, M. P. Vu, P. V. Q. Duong, K. T. Nguyen, *Langmuir* **2024**, *40*, 1698; b) H. Jang, R. Rusconi, R. Stocker, *NPJ Biofilms Microbiomes* **2017**, *3*, 6.